BULLETIN OF THE POLISH ACADEMY OF SCIENCES
TECHNICAL SCIENCES, Vol. 73(3), 2025, Article number: e153434
DOI: 10.24425/bpasts.2025.153434

Multifunctional control system to enhance the operational capability of the unmanned multirotor platform dedicated to the diagnostics of building structures

Roman CZYBA[1]*, **Jarosław DOMIN**[2], and **Marcin GÓRSKI**[3]

[1] Silesian University of Technology, Faculty of Automatic Control, Electronics and Computer Science, Gliwice, Poland
[2] Silesian University of Technology, Faculty of Electrical Engineering, Gliwice, Poland
[3] Silesian University of Technology, Faculty of Civil Engineering, Gliwice, Poland

Abstract. Drones have become common devices that are increasingly used, from toy mini drones to very advanced autonomous flying platforms used in various industries. The safety of using engineering structures and the need to shorten the time of carrying out diagnostic activities, and thus reduce costs, force the use of innovative tools to carry out an automated and unmanned process of assessing the technical condition of existing engineering structures, especially large-size ones, including bridges strengthened with external FRP (fibre reinforced polymer) composite overlays. There are conventional methods for assessing the technical condition of existing building structures conducted by inspectors and experts, involving the use of typical inspection and diagnostic tools. During the research, it was found that it is possible to conduct an automated and unmanned process of assessing the technical condition of engineering structures using an unmanned flying platform equipped with a thermal imaging diagnostic device. The uniqueness of the presented solution is that the drone is equipped with a docking module that allows the drone to be temporarily attached to the structure being diagnosed for the duration of diagnostic activities. To ensure appropriate conditions for structural diagnostics, a unique system of automated diagnostic processes and a multi-stage structure of the control system in all phases of operation were developed. The article presents a solution for the control system based on control consistent with the reference model. In particular, the focus was on the difficult and dangerous issue of altitude control during the docking phase. Simulation tests conducted in the MATLAB/Simulink environment, as well as laboratory and field tests on a real drone proved the correctness of the proposed solutions, which facilitated the undisturbed operation of the diagnostic module.

Keywords: UAV diagnostic platform; automatic control system; drone; structural health monitoring.

1. INTRODUCTION

Nowadays, drones are increasingly being used to perform a variety of tasks and have begun to conquer the market thanks to dynamic technological development. Advances in material engineering facilitate the creation of durable, lightweight structures. Similar processes are observed in the area of high-performance, energy-efficient propulsion units. Novel dedicated electronic systems with a high scale of integration at low energy consumption, high-performance power sources, high-accuracy sensor systems, or fast and efficient radio communication protocols are being developed [1–3].

UAVs (unmanned aerial vehicles) are tools that both extend the range of services offered and significantly reduce operating costs. Unmanned aerial vehicle technology has enormous potential in the field of airport security systems, among others. A single UAV can now be used to patrol an area in prevailing standard weather conditions, whereas previously, several people were responsible for its protection. It is possible to define an automatic flight path performed by the drone without an operator in certain weather conditions and assign specific tasks to be performed. A drone is also a tool that can effectively support human work while eliminating the human factor. However, the effectiveness of UAVs is not evidenced by their possession of the relevant services but by the dedicated software used in UAVs. The combination of technology, software and the lack of perception limitations typical of the human factor constitute the advantage of this technology over existing solutions.

Advanced electronics, miniaturisation of devices and the expanding range of UAV applications have explored the drone market [4, 5]. Military technologies initially stimulated the development of UAVs, but nowadays, drones also have wide civilian applications. UAVs are used in almost all sectors of the economy and many other areas. They have already become part of everyday life and are being increasingly utilised.

Drone technologies are among the most dynamically developing technologies due to their expanding range of possible applications. Among the most obvious, best-known applications are military ones. In addition, drones are used in environmental protection, agriculture, electrical power engineering,

*e-mail: roman.czyba@polsl.pl

Manuscript submitted 2023-11-23, revised 2024-12-27, initially accepted for publication 2025-01-13, published in May 2025.

mapping, aerial photography, medicine, and many other fields. Using drones for military operations is related to reducing the risk of losing soldiers and reducing the cost of military operations [6]. An important aspect of using drones for military tasks is that they are more difficult to detect by radar systems due to their flexibility of movement and relatively small size [7]. In environmental protection, unmanned aerial vehicles are used to measure air pollution [8,9]. In agriculture, drones are widely used for monitoring forest areas, monitoring forest and livestock animals, identifying them, assessing their health and tracking their migrations [10,11]. In electrical power engineering, drone applications include high-voltage line inspections and line fault detection (defects location) [12–14]. The mapping application refers to the operation of drones in acquiring images from the bird's eye view of different resolutions and 3D light and distance detection (LIDAR) point cloud data of different point densities. These tasks mainly include two aspects: data acquisition and processing [15–17]. In medicine, drones are mainly used to deliver medical supplies. During the COVID-19 pandemic, drones were used in some countries to transport defibrillators and personal protective equipment (masks, gloves and more) [18]. In some African countries, drones are used to deliver blood to health facilities and other medical supplies, such as for malaria treatment [19]. In medical transport, drones are an alternative to road transport [20].

In addition to the abovementioned, drones are also used in special, dedicated applications. One such example is a drone dedicated to the diagnostics of building structures. This solution was developed at the Silesian University of Technology in Gliwice.

The project aimed to develop a drone for inspection and diagnostics of building structures, including those strengthened with fibre-reinforced polymer (FRP) overlays, which will allow remote assessment of the risk of a construction failure. One of the most popular methods used to strengthen structures is the application of a composite FRP strengthening system. The use of FRP for the strengthening of building structures entails periodic inspections. Currently, the quality of externally bonded reinforcements of FRP is checked locally by using a pull-off test, which does not allow for a reliable assessment of the entire strengthening solution. An alternative to destructive techniques is the innovative thermal method, which allows for the evaluation of the strengthening without its disassembly. This method uses thermal techniques to evaluate the quality of the strengthening. The thermal diagnostic method, described in detail in the paper [21], facilitates using a drone for that kind of inspection.

The inspection of building structures with a drone requires a highly skilled pilot. The entire operation is divided into stages, which are described later in the paper. The use of drone technology for a variety of specialised tasks requires operators to have the proper licenses. European Union law requires registration of UAV operators whose operations may pose risks, including threats to public security, the protection of privacy and personal data or the protection of the environment.

Due to the difficult manual manoeuvres of the pilot necessary during the diagnostic process, especially the docking and undocking, a module increasing the degree of autonomy of the unmanned multi-rotor platform dedicated to the diagnostics of building structures was developed. This paper aims to present the drone automatic control system, ensuring autonomous flight, including the phase of docking, conducting the diagnostic process and undocking from the tested surface. The developed control system relieves the drone pilot from burdensome and dangerous air operations, which can be difficult to perform in direct contact with the building structure.

The paper consists of six sections. After the introduction, in Section 2, the drone design and control with a measurement system are described. In the next section, the mathematical model of a UAV with docking and heating modules is presented. The structure of the control system oriented to altitude control in the docking phase is described in Section 4. In Section 5, the simulation results, as well as the results of laboratory tests conducted using a real drone, are presented to prove the effectiveness of the proposed approach. The last section briefly discusses the results obtained and summarises and presents the novel achievements of the solutions described, which may be of relevance to other SHM (structural health monitoring) researchers and practitioners. The most important achievements presented in the work are the author's system and algorithms for controlling a multifunctional diagnostic drone, with a unique function of docking under the monitored surface of the building structure and an original diagnostic module enabling the testing of FRP strengthening quality.

2. SYSTEM CONFIGURATION

The construction of the flying platform capable of performing the diagnostic process is shown in Fig. 1.

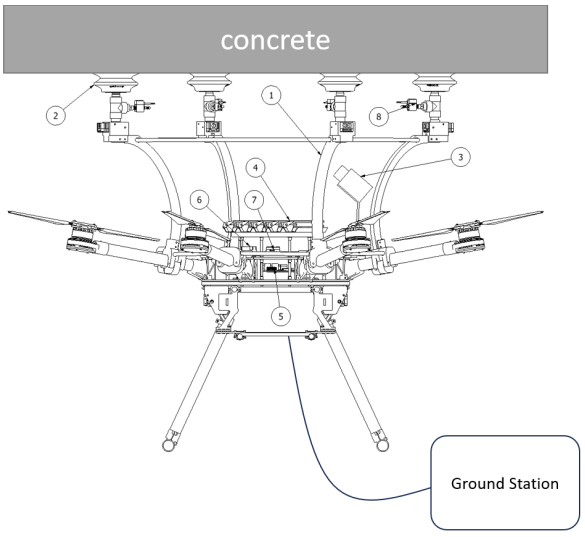

Fig. 1. Flying platform equipped with docking and diagnostic modules

The drone is equipped with a pneumatic docking module (tagged in Fig. 1 as 1) on suction cups (2) attached to the bottom surface of a hard-to-reach structural element. This tool is designed to make an inventory of structural damage using the installed inspection camera, collect the data necessary to deter-

mine the condition of the structure, and in the case of structures strengthened with FRP overlays – detach the strengthening laminate from the surface concrete element – using an IR camera (3) integrated with the filament of discharge lamps (4).

The inspection flying platform is designed in such a way that it can also be equipped with a vision camera and humidity, temperature and pH sensors, which would facilitate a comprehensive assessment of the hazards of building structures of any type. The platform could then be used not only to assess the condition of the structure but also to evaluate new buildings that are difficult to access.

The diagnostic process of a building structure with the help of a drone is divided into five stages. The most difficult stage of the diagnostic process is to attach it to the test surface and detach it from it. This process requires the pilot with high manual skills, so it is advisable to develop a module to increase the drone autonomy. For this purpose, the drone was equipped with two additional sensors: distance sensor Sharp GP2Y0A21YK0F (no. 6 in Fig. 1) and lidar TFMini Plus UART (no. 7 in Fig. 1).

The control and management system consists of three subsystems: the UAV fight control system (Pixhawk flight controller), the management system of the diagnostic process – Raspberry Pi 4 – integrated with the drone and the thermal diagnostic system at the ground station. The heart of the flight control system is the autopilot. It is an advanced controller that allows you to perform flights in manual or automatic mode. The project uses the commercially available Orange Cube flight controller (previously known as Pixhawk 2.1), which, combined with the Futaba FX20 RC apparatus, gives the operator full control during the flight of the UAV. For the presented solution, the Robotic Operating System (ROS) for communication between the Raspberry Pi and the PixHawk autopilot was used. The advantage is that the architecture of this software relies on the exchange of information between programs via messages sent using the P2P communication model. The P2P model uses the MavLink communication protocol to exchange data with PixHawk. In addition, the MavROS library was used, which has an API (application programming interface) that allows for easy data exchange. The diagnostic process management system is used to manage the heating module (4), pneumatic docking module (1), vacuum sensors (8), distance sensor (6), lidar (7) and IR camera.

The thermal measurement data are sent to the ground station, where they are processed and analysed. The control and measurement system are graphically presented in Fig. 2.

The diagnostic process consists of sequential steps that the platform performs autonomously. The drone operator flies under the tested surface at a distance of est. 1 m.

The diagnostic procedure starts when the button on the RC apparatus is activated. The diagnostic process is fully automatic from the start of the diagnostic procedure. The process ends when the drone returns to the starting position. When returning to the starting position, the operator takes control of the flight and can move to another place and make further measurements. The entire diagnostic process is performed automatically, including the following stages:

- Stage I – approaching the designated point of the structure and sucking to the surface.

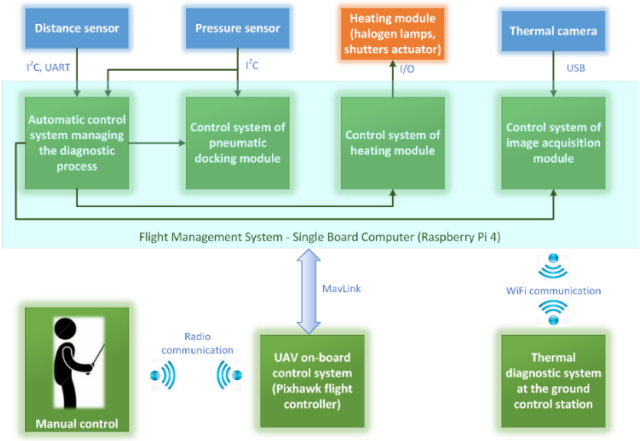

Fig. 2. Block diagram of the control and measurement system

- Stage II – turning off the motors in a free hover state.
- Stage III – heating the surface and thermographic data acquisition.
- Stage IV – increase engine speed and return to weight balance.
- Stage V – detach and return to the starting position.

3. MATHEMATICAL MODEL OF A UAV WITH DOCKING AND HEATING MODULES

Significant complexity of phenomena found in UAV flight results in highly nonlinear processes. This section presents the UAV mathematical model, which reflects its most significant behaviours. Details related to the modelling of the UAV platform and identification of the propulsion system are presented in [22]. The mathematical model of the multirotor is intended to create a simulation environment for testing the designed system that increases the degree of autonomy of the UAV during the diagnostic procedure. Due to the complexity of the system, it is necessary to make the following assumptions simplifying the model [23]:

- The model is a rigid body (no blade flipping).
- The structure of the model is symmetrical.
- The centre of drone gravity is located at the centre of the intersection of the multirotor frame arms.
- Due to the installation of additional accessories - the docking module and the heating module – the centre of gravity is shifted along the z-axis of the assumed coordinate system, thus worsening its flight characteristics and reducing the stability margin.

The design uses an eight-rotor platform known as an octorotor (Fig. 3). The propellers (1, 3, 5, 7) rotate clockwise, and the propellers (2, 4, 6, 8) rotate counterclockwise. To describe the mathematical model, two coordinate systems are specified. The first coordinate system F_E is related to the earth and is described by the ENU (East North Up) coordinate system. The second coordinate system F_F is related to the multirotor frame and is located at its centre of gravity. The directions of rotation of the Euler angles Φ, θ, Ψ, which are related to the roll, pitch and yaw of the octorotor, respectively, are marked in Fig. 3.

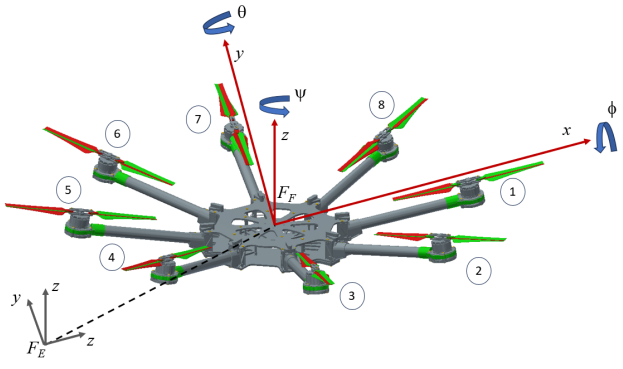

Fig. 3. Octorotor configuration and coordinate systems

The multirotor platform is described by 12 state variables.

$$\bar{x} = \left[p, q, r, \Phi, \theta, \Psi, x, y, z, \dot{x}, \dot{y}, \dot{z}\right]^T, \tag{1}$$

where p, q, r – angular velocities of the platform around three orthogonal axes; Φ, θ, Ψ – Euler angles; x, y, z – linear displacement in individual axes; $\dot{x}$, $\dot{y}$, $\dot{z}$ – velocities along x, y, z axes.

The translational and rotational motion of the multirotor is described by the following equations [23–25]

$$\dot{p} = \frac{I_{yy} - I_{zz}}{I_{xx}} qr + \frac{\tau_\Phi + \tau_{\Phi\text{prec}}}{I_{xx}}, \tag{2}$$

$$\dot{q} = \frac{I_{zz} - I_{xx}}{I_{yy}} pr + \frac{\tau_\theta + \tau_{\theta\text{prec}}}{I_{yy}}, \tag{3}$$

$$\dot{r} = \frac{I_{xx} - I_{yy}}{I_{zz}} pq + \frac{\tau_\Psi}{I_{zz}}, \tag{4}$$

$$\dot{\Phi} = p + q\tan\theta\sin\Phi + r\tan\theta\cos\Phi, \tag{5}$$

$$\dot{\theta} = q\cos\Phi - r\sin\Phi, \tag{6}$$

$$\dot{\Psi} = q\frac{\sin\Phi}{\cos\theta} - r\frac{\cos\Phi}{\cos\theta}, \tag{7}$$

$$\ddot{x} = \frac{\sin\Psi\sin\Phi + \cos\Psi\sin\theta\cos\Phi}{m}\sum_{i=1}^{n} F_i, \tag{8}$$

$$\ddot{y} = \frac{-\cos\Psi\sin\Phi + \sin\Psi\sin\theta\cos\Phi}{m}\sum_{i=1}^{n} F_i, \tag{9}$$

$$\ddot{z} = -g + \frac{\cos\theta\cos\Phi}{m}\sum_{i=1}^{n} F_i, \tag{10}$$

$$F_i = b\Omega_i^2, \tag{11}$$

$$\tau_\Phi = b\sum_{i=1}^{n} lx_i\Omega_i^2, \tag{12}$$

$$\tau_\theta = b\sum_{i=1}^{n} ly_i\Omega_i^2, \tag{13}$$

$$\tau_\Psi = d\sum_{i=1}^{n} \Omega_i^2(-1)^{(i-1)}, \tag{14}$$

$$\tau_{\text{prec}} = \begin{bmatrix} \tau_{\theta\text{prec}} \\ \tau_{\Phi\text{prec}} \\ 0 \end{bmatrix} = \begin{bmatrix} -J_r q\sum_{i=1}^{n}\Omega_i(-1)^{(i-1)} \\ J_r p\sum_{i=1}^{n}\Omega_i(-1)^{(i-1)} \\ 0 \end{bmatrix}, \tag{15}$$

where I_{xx}, I_{yy}, I_{zz} – moments of inertia around x, y, z axes, respectively; τ_Φ, τ_Θ, τ_Ψ – torques acting around the x, y, z axes, respectively; τ_{prec} – precession (gyroscopic effect); F_i – thrust generated by the i-th rotor; n – number of rotors (in our case $n = 8$); b – thrust coefficient; d – drag coefficient; lx_i, ly_i – the distance from the i-th rotor to the centre of gravity projected on the x and y axes; Ω_i – rotational speed of the i-th rotor; g – gravitational force; m – mass; J_r – rotor inertia (motor and propeller).

The presented equations of motion describe each multi-rotor configuration; however, thrust and torque must be modified accordingly. The first step in determining the thrust and its effect for a given multirotor configuration was to calculate the distance of the motor from the given axis.

It is possible to determine the direction of rotation in a given axis based on the position of the motor in the quadrants of the system by utilising Fig. 4 [24].

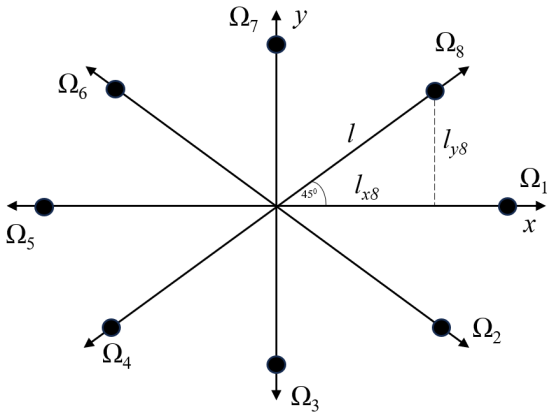

Fig. 4. Determination of the distance between the motors and the axis of rotation

The next step in creating the model was to determine the moments of inertia, mass, arm length, motor inertia, thrust and drag coefficient, as well as the time constant and gain of the motor model. The Autodesk Inventor environment was used to determine the moment of inertia. Docking and heating modules were added to the drone model, along with material parameters, as shown in Fig. 1. The determined physical parameters and other parameters of the model are included in Table 1.

The block diagram of the octorotor is shown in Fig. 5.

The inputs to the system are signals that control the rotation angles of the octorotor around the x, y, z axes (u_Φ u_θ u_Ψ) and the altitude through the thrust control signal (u_T). These signals form the following control vector

$$\bar{u} = \left[u_T, \quad u_\Phi, \quad u_\Theta, u_\Psi\right]^T. \tag{16}$$

Table 1
Octocopter parameters

Parameter	Symbol	Value	Unit
Mass	m	10.34	kg
Moment of inertia of the x-axis	I_xx	0.1598	kg·m^2
Moment of inertia of the y-axis	I_yy	0.248	kg·m^2
Moment of inertia of the z-axis	I_zz	0.1671	kg·m^2
Moment of inertia	I_xy	–3.077E-6	kg·m^2
Moment of inertia	I_xz	1.495E-6	kg·m^2
Moment of inertia	I_yz	–0.24E-3	kg·m^2
Thrust coefficient	b	3.13E-5	N·m^2
Arm length	l	0.386	m
Rotor inertia	J_r	6, 00E-5	kg·m^2
Drag coefficient	d	7.5E-7	N·m·s^2
Rotor gain	k_r	0.936	–
Time constant	T	0.178	s

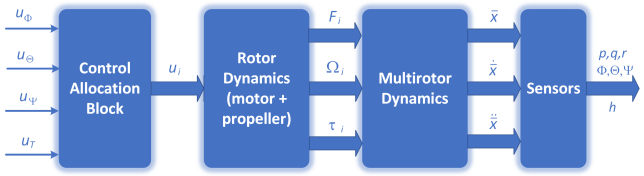

Fig. 5. Block diagram of a multirotor syste

In the control allocation block, the distribution of control signals to individual rotors, depending on the vector of control signals, is determined. The control signal for the i-th rotor is described by the following relationship [23]

$$u_i = u_T - u_\theta \cos\frac{2\pi(i-1)}{n} - u_\Phi \sin\frac{2\pi(i-1)}{n} + (-1)^i u_\Psi . \quad (17)$$

The rotor is treated as one module consisting of a BLDC (brushless direct-current) motor, a propeller and an ESC (electronic speed controller) with a PWM (pulse width modulation) control signal. A first-order transfer function describes the dynamics of the rotor

$$K(s) = \frac{\Omega_i(s)}{U_i(s)} = \frac{k_r}{Ts+1}, \quad (18)$$

where k_r – rotor gain; T – time constant of the rotor (depending on motor response time and propeller inertia).

The measurement system consists of two subsystems:

- Classic, directly related to the flight and built into the autopilot system, which includes the AHRS system, GPS, and pressure sensor.
- Dedicated to the docking task, and that is what we will now focus on.

In the docking process, the key issue is the precise measurement of the distance from the target suction surface – in this case, it is the lower surface of the concrete bridge span. An important parameter is the distance to the surface itself, which must be continuously monitored. Two sensors were used in the project: the first is the Sharp GP2Y0A21YK0F analogue sensor, which measures with high accuracy but allows the detection of objects at a short distance of 0.1 to 0.8 m; the second one is the Lidar TFMini Plus laser sensor, operating in the range from 0.1 to 12 m. The choice of two complementary distance sensors allows increasing accuracy over the entire measuring range of 0.1 m – 12 m. The first sensor is more accurate for short distances, and the second for long distances. A single distance measurement result is possible thanks to the data fusion achieved based on the complementarity of measurements. For this purpose, functions $a(d_1)$ and $b(d_2)$ were created for each sensor individually, determining the value of the normalised "reliability coefficient" depending on the measured distance. Their values are presented graphically in Fig. 6.

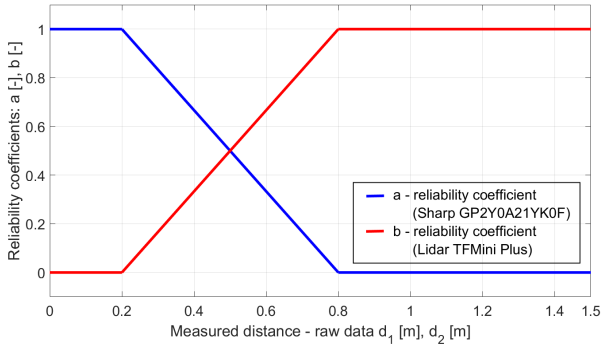

Fig. 6. Values of reliability coefficients as functions of distance

Distance measurement is divided into three zones:

- Up to 0.2 m, where the distance is determined by the Sharp short-distance sensor.
- From 0.2 m to 0.8 m, where the importance of sensors changes.
- From 0.8 m to 12 m, where the distance is determined using the Lidar long-distance sensor.

The distance is determined according to the relation below

$$D = D(d_1, d_2) = \frac{a(d_1)}{a(d_1)+b(d_2)} \cdot d_1 + \frac{b(d_2)}{a(d_1)+b(d_2)} \cdot d_2 , \quad (19)$$

where $a(d_1)$ – reliability coefficient of the short-distance sensor, $b(d_2)$ – reliability coefficient of the long-distance sensor, d_1 – a measured value of the short-distance sensor, d_2 – a measured value of the long-distance sensor.

The distance value determined in this way is used during the platform docking manoeuvre to the object on which the diagnostics are performed.

In the presented mathematical model of the UAV, the value of the thrust force of a given rotor is a nonlinear function of its rotational speed (equation (11)), while the dependence of the rotational speed on the control signal is described by equation (18) (first-order inertia). The rotor is treated as one module consisting of the ESC (electronic speed controller), engine and propeller. The control signal for each ESC is the PWM signal (cPPM in the newer implementation) and this is our control signal in equations (17) and (18). The ESC system is responsible

for mapping the PWM signal to phase currents controlling the motor. This is an off-the-shelf technical solution that is standard in all UAV drives.

The entire control system design process was an iterative process that was conducted based on the MBD (model-based design) method, using the rapid prototyping methodology in the controller tuning process. The starting point was the simulation model described in the article and the default controller settings provided by the commercial manufacturer of the Orange Cube flight controller used in our project. The structural changes introduced to our platform (attached diagnostic and docking modules) resulted in the need to improve the regulator settings. In tuning individual controllers, a method of closing subsequent regulatory loops was used. After tuning the controllers in off-line simulation conditions, online testing began on a real platform in conditions similar to the future operation of the device. In real tests, the controller settings were adjusted iteratively, each time making appropriate corrections in the simulation model.

4. CONTROL SYSTEM STRUCTURE

The general structure of the control system (Fig. 7) consists of two subsystems: the first one is attitude stabilisation around hovering conditions, and the second is altitude regulation.

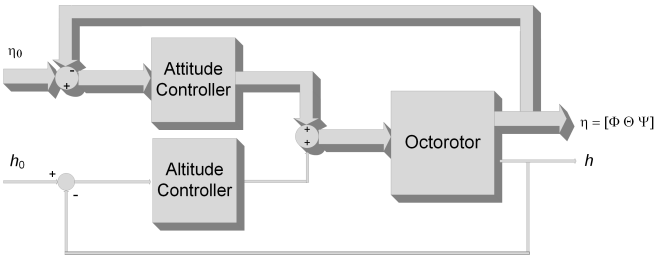

Fig. 7. Block diagram of the control system

A comprehensive discussion on the attitude stabilisation system can be found in [26].

The next section focuses on the issue of altitude control during the docking phase.

4.1. Statement of control problem

To design an altitude controller for the docking procedure let us consider a nonlinear time-varying SISO system in the following form

$$\bar{x}^{(1)}(t) = \bar{w}\left(\bar{x}(t), u(t), t\right), \quad \bar{x}(0) = \bar{x}_0, \tag{20}$$

$$y(t) = g\left(\bar{x}(t), t\right), \tag{21}$$

where $\bar{x}(t)$ is the n-dimensional state vector, $y(t)$ is an output and $u(t)$ is the control input. The elements of $\bar{w}\left(\bar{x}(t), u(t), t\right)$ and $g\left(\bar{x}(t), t\right)$ are differentiable functions.

Output $y(t)$ can be differentiated m times until the control input appears. This leads to the following equation

$$y^{(m)}(t) = f\left(\bar{x}(t), t\right) + b\left(\bar{x}(t), t\right) u(t), \tag{22}$$

where $0 < b(\bar{x}(t), t) \leq b^{\max}$, $\|f(\bar{x}(t), t)\| \leq f^{\max}$.

In this case, the value $y^{(m)}$ depends explicitly on the input $u(t)$. The value m is a relative order of the system (21) and (22) concerning the output $y(t)$ (or so-called the order of a relative higher derivative).

The differential equations (2)–(18)), presented in the section dedicated to the UAV mathematical model, provide basic information about the drone dynamics and, thus, about the relative order of the system.

The approach to docking the drone should be smooth without overshooting. Otherwise, the docking module may be damaged. In the control system with the controller containing the integral action and without protection in the form of the anti-windup system, overshoot in combination with a rigid spatial limitation in the form of the bridge surface may lead to the destruction of the drone. Therefore, in this work, a control in accordance with the reference model was introduced, thanks to which it is possible to define the aperiodic character of the docking process.

The significant feature of this approach is that the control problem was stated as a problem of determining the root of an equation by introducing a reference differential equation whose structure complies with the structure of the plant model equations. Thus, the control problem can be solved only if the behaviour of the $y^{(m)}$ fulfils the reference model, which is given in the form of the following stable differential equation

$$y_M^{(m)}(t) = F_M\left(\bar{y}(t), r(t)\right), \tag{23}$$

where F_M is called the desired dynamics of $y(t)$, $\bar{y}_M(t) = \left[y_M, y_M^{(1)}, \ldots, y_M^{(m-1)}\right]^T$, $r(t)$ is the reference value, and the condition $y = r$ takes place at an equilibrium point.

The reference value can be either at the constant level above the ground or a trajectory defined for docking and undocking manoeuvres. Thus, equation (23) has a form of linear differential equation

$$y_M^{(m)}(t) = -\sum_{i=0}^{m-1} \alpha_i y^{(i)} + \sum_{j=0}^{n} \beta_j r^{(j)}, \tag{24}$$

where α_i, β_j are constant coefficients and $m \geq n$.

Let us denote

$$\Delta^F = F_M\left(\bar{y}(t), r(t)\right) - y^{(m)}(t), \tag{25}$$

where Δ^F is the error of the desired dynamics realisation.

As a result of (20)–(25), the behaviour of $y(t)$ will be provided if the following condition is fulfilled

$$\Delta^F\left(\bar{x}(t), y(t), r(t), u(t), t\right) = 0. \tag{26}$$

The solution to the control problem (26) is based on the application of the higher order output derivatives jointly with high gain in the controller. Control law in the form of a stable differential equation is constructed in such a way that its stable equilibrium is the solution of equation (26). Such an equation can be presented in the following general form [26]

$$\mu^q u^{(q)} + \sum_{j=0}^{q-1} \mu^j d_j u^{(j)} = k\Delta^F, \quad u(0) = u_0, \tag{27}$$

where $u(t)$ is controller output, μ is a small positive parameter, $d_0, \ldots, d_{q-1}$ controller parameters and k is gain.

Considering equations (23), (24) and (27), the following dynamic control law was obtained

$$\mu^q u^{(q)} + \sum_{j=0}^{q-1} \mu^j d_j u^{(j)} = k \left[\sum_{j=0}^{n} \beta_j r^{(j)} - \sum_{i=0}^{m} \alpha_i y^{(i)} \right]. \quad (28)$$

Remark 1. It is assumed that the relative order of the system (20), (21), determined in (22), and the order of the controller equation (28) is the same as m.

Remark 2. Assuming that $q \geq m$, then, the control law (28) is proper.

Remark 3. Assuming that $d_0 = 0$ in equation (28), the controller includes integration, and it provides that the closed-loop system is type I with respect to the reference signal.

Remark 4. To determine the order m of the reference model, the knowledge of drone dynamics is required.

4.2. Altitude control in the docking phase

The control law in the form of (28) facilitates the creation of desired output dynamics for nonlinear and nonstationary plants despite incomplete information about the possible changes in system parameters and external disturbances. Despite its many advantages, there are also some drawbacks. Calculation of the output derivatives could cause problems. This paper proposes a modification of the control law (28). Namely, if it is possible to measure signals, which are derivatives of the process variable, or if it is possible to estimate the required signals, then we can use them directly in the control loop. Modification of the control law (28) relies on the replacement of higher derivatives in the controller through the multi-loop (cascade) system with lower-order controllers for respective signals, which are the derivatives of the process variables. Equation (28), containing the higher order output derivatives, was decomposed into a set of differential equations at most second. This approach reduces the problem, presented in Section 4.1, to structural design with higher-order derivatives in feedback. The proposed modification can be presented in the following general form

$$u_T = h_0 \left(\prod_{j=0}^{m} K_{R,j} \right) - \sum_{i=0}^{m} h^{(i)} \left(\prod_{j=1}^{m} K_{R,j} \right), \quad (29)$$

where $K_{R,j}$ controller in j-th control loop, m – relative order of the system.

In a generalisation, KR, J has the following form

$$\mu^2 u_T^{(2)} + \mu d_1 u_T^{(1)} + d_0 u_T = k \left[\sum_{j=0}^{2} \beta_j h_0^{(j)} - \sum_{i=0}^{2} \alpha_i h^{(i)} \right]. \quad (30)$$

The advantages of this approach are:

- The order of individual controllers is relatively low.
- Parameters of the first and second dynamical systems have very well-known physical meanings, and their particular values can be easily specified.
- There is ease of implementation, rapid prototyping of particular controllers and commissioning of the whole control system.

The idea of structural design with higher derivatives in feedback loops is depicted in Fig. 8.

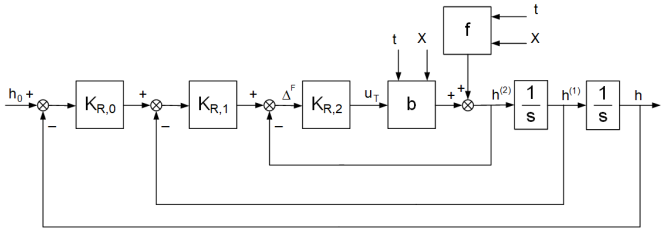

Fig. 8. An idea of structural design with higher derivatives in feedback loops

5. FLIGHT TESTS AND RESULTS

The tests were divided into two stages. The first stage aimed to verify through simulation the correct operation of the designed control system module of the automatic diagnostics procedure of the bridge surface strengthened with the FRP composite overlay. In the second stage, the effectiveness of the designed control system was verified in laboratory tests of a real drone.

5.1. Test results in a simulation environment

Simulation of the diagnostic process is the first stage of examining the platform behaviour after increasing the autonomy of the unmanned multi-rotor platform dedicated to the diagnostics of bridge structures. Flight analysis in the simulation is a safe form of testing and is devoid of consequences as a result of failure. The tests were conducted in the MATLAB/Simulink environment.

A dangerous stage of the diagnostic process is the moment of touch and detachment from the analysed surface. Approaching the tested surface at too high a speed may cause the docking module to hit the surface, which creates a real threat to flight stability and may cause damage to the docking module and the structure of the entire platform. The control system must fulfil several criteria: the system must be stable, provide a type I system, and ensure zero overshoot when approaching the test surface.

In the designed system, the control task is conducted in accordance with a predefined reference model. According to (23) and (30), the reference model is a second-order low-pass filter. The parameters were selected so that the response of the reference model was aperiodic (Fig. 9). In the simulation, it was assumed that the platform was in the centre of the coordinate system at a height of 3 m and the distance from the surface was 1 m.

Figure 10 shows the position of the flying platform on the z-axis during the entire diagnostic process, performed automatically, including all stages. The response of the system coincides

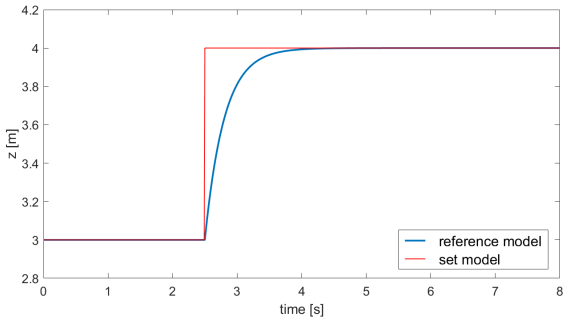

Fig. 9. Reference model response

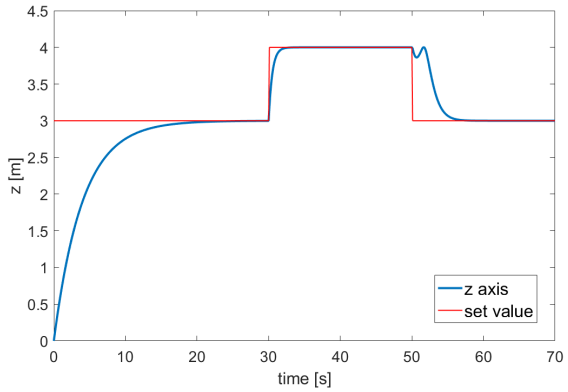

Fig. 10. Position of the platform in the z-axis

with the reference model. The common control signal of all motors is shown in Fig. 11. Two critical moments during the entire process, namely the suction stage and the detach stage, are shown in Fig. 12 and Fig. 13, respectively.

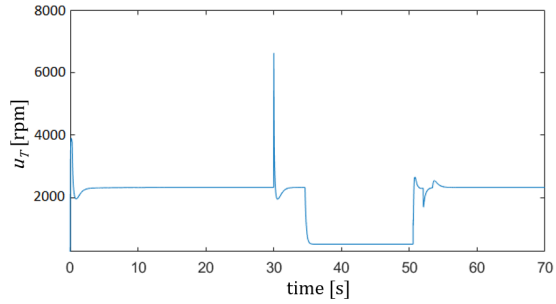

Fig. 11. Common control signal

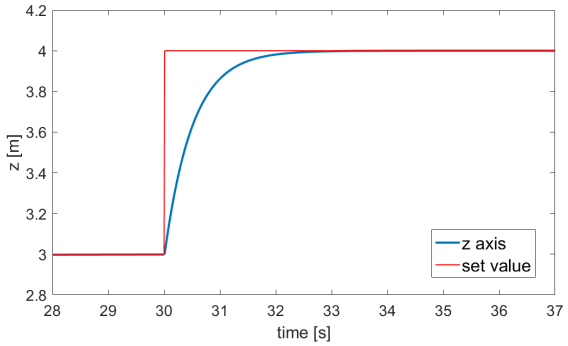

Fig. 12. Stage I – docking the drone to the surface

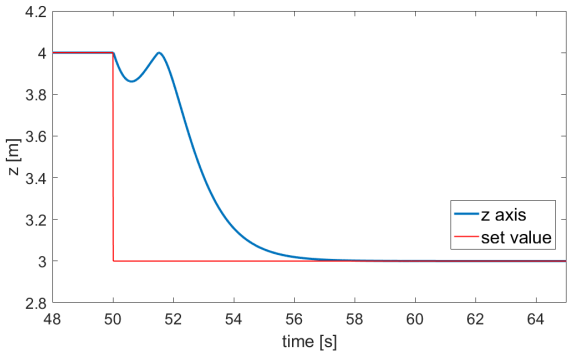

Fig. 13. Stage V – detaching the drone from the surface

5.2. Test results in a simulation environment

After mounting the pneumatic docking module and the heating module on the flying platform, the first tests with a real drone were conducted on a reinforced concrete slab in the laboratory at the Faculty of Civil Engineering of the Silesian University of Technology. During laboratory and in situ tests, different types of surfaces on which the drone docked were tested. The variability included surface roughness, defects, cleanliness and slope. After several trials in which uneven pressure in the suction cups was noticed, a proprietary suction control algorithm was developed to equalise the pressures, eliminating the observed problem and allowing standard conditions for a safe take-off. The entire diagnostic process covering all five stages was successfully conducted. Figure 14 shows the drone after docking to the structure, while Fig. 15 shows the heating phase of the tested

Fig. 14. Drone after docking to the surveyed surface

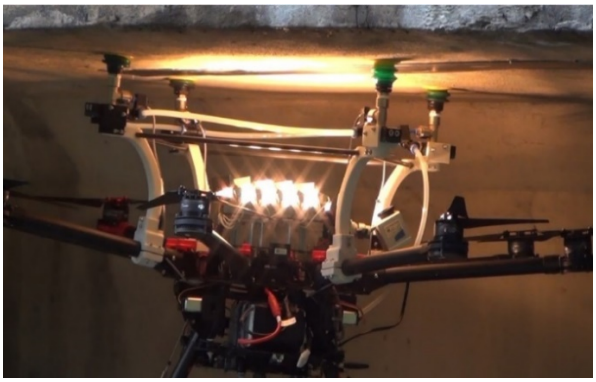

Fig. 15. Diagnostics – warm-up phase

surface. The test confirmed the correctness of the operation of the automatic control system managing the diagnostic process.

6. CONCLUSIONS

The paper presents an automation solution for a unique UAV-based device specialised in diagnosing building structures, particularly those strengthened with external FRP overlays. The main aim of this paper was to develop and design the drone automatic control system, ensuring autonomous flight, including the docking phase, conducting the diagnostic process, and undocking from the tested surface.

The device carries the original diagnostic module to verify the degree of integration of the FRP strengthening solution with the concrete surface. This module uses the thermographic technique consisting of a thermal imaging camera and a heating module. Both the heating module and the thermographic device require considerable proximity to the structure for the time of the local examination. The quality of the reading, which can be considered dependable, requires uninterrupted operation of the diagnostic module. The above premises influenced the construction of a drone with the possibility of docking on the bottom surface of the building structure. A complex system of controlling the free flight phase, the process of approaching the structure, docking on various types of surfaces, turning the engines off, performing diagnostic tests and then undocking and free flight to the next diagnostic location, required the development of a unique structure of dedicated control system.

Such a control system was elaborated analytically, based on theoretical assumptions, and confirmed then in a numerical environment. In this paper, the issue of altitude control in the difficult phase of docking to a building structure was discussed in detail. The developed control law is based on control consistent with the reference model and leads to a structural design that involves replacing higher derivatives in the controller with a multi-loop system with simpler controllers, at most second order, for appropriate signals that are derivatives of the process variable. These solutions were improved after assessing the diagnostic drone in laboratory conditions and verified in field tests on several types of building structures, including a real bridge structure. The tests confirmed the legitimacy of the adopted solutions. The developed structure results in sudden and fast control when a disturbance occurs in the control loop. This important property will be used in control during emergencies, such as suction cup detaching, which will be the topic of subsequent research.

ACKNOWLEDGEMENTS

This research was co-financed by the European Union thanks to the support of projects: POWER-03.05.00-00-Z098/17-00 and "Innovation Incubator 2.0: Support for scientific research management and commercialisation of R&D results in scientific units and enterprises" under the Smart Growth Operational Program 2014-2020 (Measure 4.4) GA: RJO4/2019/II2.0-01 implemented at the Silesian University of Technology (SUT). This work was also financed in part by a grant from SUT – a subsidy for maintaining and developing the research potential in 2025.

REFERENCES

[1] I.A. Raptis and K.P. Valavanis, "Linear and Nonlinear Control of Small-Scale Unmanned Helicopters," in *Intelligent Systems, Control and Automation: Science and Engineering*, vol. 45. London, Springer, 2011, doi: 10.1007/978-94-007-0023-9.

[2] K.P. Valavanis, "Advances in Unmanned Aerial Vehicles," in *Intelligent Systems, Control and Automation: Science and Engineering*, vol. 33. Springer, Netherlands, 2007, doi: 10.1007/978-1-4020-6114-1.

[3] P. Szywalski and A. Waindok, "A decentralized radio network for small groups of Unmanned Aerial Vehicles," *Bull. Pol. Acad. Sci. Tech. Sci.*, vol. 72, p. e147922, 2024, doi: 10.24425/bpasts.2023.147922.

[4] K. Nonami, F. Kendoul, S. Suzuki, W. Wang, and D. Nakazawa, "Autonomous flying robots" in *Unmanned aerial vehicles and micro aerial vehicles*, Springer Japan, 2010, pp. 1–329, doi: 10.1007/978-4-431-53856-1.

[5] W. Mclean, "Drones are cheap, soldiers are not: a cost-benefit analysis of war," The Conversation US, [Online]. Available: https://theconversation.com/drones-are-cheap-soldiers-are-not-a-cost-benefit-analysis-of-war-27924 [Accessed: June 26, 2014].

[6] A.Y. Husodo, N. Alfiany, G. Jati, and W. Jatmiko, "Intruder Drone Localization Based on 2D Image and Area Expansion Principle for Supporting Military Defence System," in *Proc. IEEE International Conference on Communication, Networks and Satellite (Comnetsat)*, 2019, pp. 35–40, doi: 10.1109/COMNETSAT.2019.8844103.

[7] S.N. Shah and X. Xiong, "Balluino, High Altitude Balloon/Drone Based Air Pollution and PM 2.5 Monitoring System," in Proc. *IEEE Long Island Systems, Applications and Technology Conference (LISAT)*, 2019, doi: 10.1109/LISAT.2019.8817337.

[8] J. Wivou, L. Udawatta, A. Alshehhi, E. Alzaabi, A. Albeloshi, and S. Alfalasi, "Air Quality Monitoring for Sustainable Systems via Drone Based Technology," in *Proc. IEEE International Conference on Information and Automation for Sustainability (ICIAfS)*, 2016, doi: 10.1109/ICIAFS.2016.7946542.

[9] J.T.C. Marcos and S.W. Utete, "Animal Tracking within a Formation of Drones," in *Proc. IEEE 24th International Conference on Information Fusion (FUSION)*, 2021, doi: 10.23919/FUSION49465.2021.9626844.

[10] X. Li and L. Xing, "Reactive Deployment of Autonomous Drones for Livestock Monitoring Based on Density-based Clustering," in *Proc. IEEE International Conference on Robotics and Biomimetics (ROBIO)*, 2019, pp. 2421–2426, doi: 10.1109/ROBIO 49542.2019. 8961763.

[11] T. Mao *et al.*, "Defect Recognition Method Based on HOG and SVM for Drone Inspection Images of Power Transmission Line," in *Proc. International Conference on High Performance Big Data and Intelligent Systems (HPBD&IS)*, 2019, pp. 254–257, doi: 10.1109/ HPBDIS.2019.8735466.

[12] L. Dong *et al.*, "Intelligent Inspection Method for Overhead Line Drones Supported by Hybrid Networking," in *Proc. 2nd International Conference on Algorithms, High Performance Computing and Artificial Intelligence (AHPCAI)*, 2022, pp. 542–546, doi: 10.1109/AHPCAI57455.2022.10087394.

[13] A. Hatibovic and P. Kádár, "The application of autonomous drones in the environment of overhead lines," in *Proc. IEEE 18th International Symposium on Computational Intelligence and Informatics (CINTI)*, 2018, pp. 289–294, doi: 10.1109/CINTI.2018.8928234.

[14] S. Rachmawati *et al.*, "Application of Drone Technology for Mapping and Monitoring of Corn Agricultural Land," in *Proc. International Conference on ICT for Smart Society (ICISS)*, 2021, doi: 10.1109/ICISS53185.2021.9533231.

[15] J. Wallerman, J. Bohlin, M.B. Nilsson, and J.E.S. Franssen, "Drone-Based Forest Variables Mapping of ICOS Tower Surroundings, IGARSS," in *Proc. IEEE International Geoscience and Remote Sensing Symposium*, 2018, pp. 9003–9006, doi: 10.1109/IGARSS.2018.8518895.

[16] M. Yusuf *et al.*, "Mapping of Salt field using Drone for Geographic Information System (GIS)," in *Proc. IEEE 8th Information Technology International Seminar (ITIS)*, 2022, pp. 241–245, doi: 10.1109/ITIS57155.2022.10010193.

[17] E. Ackerman and E. Strickland, "Medical delivery drones take flight in east Africa," *IEEE Spectrum*, vol. 55, pp. 34–35, 2018, doi: 10.1109/MSPEC.2018.8241731.

[18] M.J. van Veelen, M. Kaufmann, and H. Brugger, "Drone delivery of AED's and personal protective equipment in the era of SARS-CoV-2," *Resucitation*, vol. 152, pp. 1–2, 2020, doi: 10.1016/j.resuscitation.2020.04.038.

[19] K.G. Lakshmi, P. Kumar, M. Rishitha, G.N. Swamy, and T.A. Kumar, "Innovative Usage Of Drones In Medical Emergency," in *Proc. 9th International Conference on Advanced Computing and Communication Systems (ICACCS)*, 2023, pp. 409–414, doi: 10.1109/ICACCS57279.2023.10112949.

[20] W. Adamczyk *et al.*, "Application of numerical procedure for thermal diagnostics of the delamination of strengthening material at concrete construction," *Int. J. Numer. Methods Heat Fluid Flow*, vol. 30 no. 5, pp. 2655–2668, 2019 doi: 10.1108/HFF-04-2019-0278.

[21] A.G. Sidea, "General model and control of an n rotor helicopter," *J. Phys. Conf. Ser.*, vol 570, pp. 1–12, 2014, doi: 10.1088/1742-6596/570/5/052004.

[22] G. Szafrański, R. Czyba, and M. Błachuta, "Modeling and Identification of Electric Propulsion System for Multirotor Unmanned Aerial Vehicle Design," in *Proc. IEEE Int. Conference on Unmanned Aircraft Systems (ICUAS)*, 2014, pp. 470–476, doi: 10.1109/ICUAS.2014.6842287.

[23] J. Fogelberg, *Navigation and Autonomous Control of a Hexacopter in Indoor Environments*, Lund, Media-Tryck, 2013.

[24] R. Josselson, *Introduction to 6-DOF simulation of air vehicles*, Boston, ITT Aerospace Systems Group, 1997.

[25] L. Wang, Z. Zhang, Q. Zhu, and Z. Wen, "Longitudinal automatic carrier-landing control law rejecting disturbances and coupling based on adaptive dynamic inversion," *Bull. Pol. Acad. Sci. Tech. Sci.*, vol. 69, no. 1, p. e1362172021, doi: 10.24425/bpasts.2020.136217.

[26] V.D. Yurkevich, *Design of Nonlinear Control Systems with the Highest Derivative in Feedback*, World Scientific Publishing, 2004.